Numerical derivation of CPT-based *p-y* curves for piles in sand

S.K. Suryasentana BEng[1]

B.M. Lehane[2] BE, MAI, DIC, PhD, FIEAust,CPEng

[1] Graduate Geotechnical Engineer

Rio Tinto Northparkes

Parkes, NSW 2870, Australia

formerly The University of Western Australia.

35 Stirling Highway, Crawley WA 6009 , Australia

[2] Corresponding Author

Professor, School of Civil & Resource Engineering

The University of Western Australia.

35 Stirling Highway, Crawley WA 6009, Australia

E-mail: *Barry.Lehane@uwa.edu.au*

Abstract

The formulations for the lateral load-displacement (*p-y*) springs conventionally used for the analysis of laterally loaded piles have been based largely on the back-analysis of the performance of small scale instrumented piles subjected to lateral load. Although such formulations have been employed with much success in Industry, their applicability to large diameters piles, such as those used to support offshore wind turbines, is uncertain and has necessitated further research in this area. Moreover, with the growth in popularity of in-situ Cone Penetration Tests (CPTs), there are demands for a theoretically supported direct method that can enable the derivation of *p-y* curves from the CPT end resistance (q_c). In this paper, a numerical derivation of CPT-based *p-y* curves applicable to both small and large diameter laterally loaded single piles in sand is presented. Three-dimensional finite element analyses were performed using a non-linear elasto-plastic soil model to predict the response of single piles in sand subjected to lateral loads. The corresponding CPT q_c profile was derived using the same soil constitutive model via the cavity expansion analogue. An extensive series of computations of the lateral pile response and CPT q_c values is then employed to formulate a direct method of constructing *p-y* curves from CPT q_c values. The proposed method is shown to be generally consistent with existing empirical correlations and to provide good predictions to the measurements obtained during lateral load tests on instrumented piles in an independent case study.

Keywords

Lateral piles, CPT, p-y curves, Load-transfer

Introduction

The *p-y* method is the most commonly employed approach to analyse the behaviour of piles subjected to lateral loads. This method idealizes the soil as a series of independent springs distributed along the pile length. The springs are assumed to be approximately independent as the width of a pile is generally much smaller than its length (Vesic 1961). Each spring has its own load-transfer relationship known as the *p-y* curve, where *p* is the soil resistance force per unit pile length and *y* is the local pile deflection.

The most widely used design method for deriving *p-y* curves in sand is the API method (American Petroleum Institute, 2011). This method evolved from the seminal paper of Reese *et al.* (1974) who compiled results from lateral tests on relatively small piles. The most recent version of the recommendations is based on the interpretation of O'Neill & Murchison (1983). These recommendations adopt a hyperbolic tangent form for the *p-y* curve and the only input parameter required is the sand's peak friction angle (ϕ'). The high sensitivity of the formulation to the selected ϕ' value is, however, problematic given the difficulties faced by geotechnical practitioners who need to employ an in-situ test such as the Standard Penetration Test (SPT) or Cone Penetration Test (CPT) to assess the sand density and hence friction angle.

The difficulties in selecting appropriate stiffness and strength parameters for the prediction of lateral pile response has prompted some research into the development of a *p-y* formulation involving direct input of an in-situ test parameter. Houlsby & Hitchman (1988)

have confirmed through experiments that the CPT end resistance (q_c) is affected significantly by the in-situ horizontal stress (σ'_{h0}) while studies of Salgado & Randolph (2001), amongst others, show that numerical predictions for q_c value depend on σ'_{h0}, ϕ' and the sand's stiffness characteristics. It is therefore plausible that the response of sand adjacent to a laterally load pile correlates, at least in an approximate way, with the CPT q_c value. Lee *et al.* (2010) explore the dependence on q_c of ultimate resistance in a numerical study entailing the numerical evaluation of q_c for sands with a variety of relative densities and in-situ stress states. These q_c values were then compared with the expression for limiting stress (P_u) proposed by Broms (1964) to deduce the following relationship between P_u and q_c value in silica sands (where p' is the mean effective stress and p_a is a reference stress=100kPa):

$$P_u = 0.196\, q_c^{0.47}\, p'^{0.63}\, p_a^{-1.1} \qquad (1)$$

Novello (1999) and Dyson & Randolph (2001) have proposed empirical CPT-based *p-y* formulations for calcareous sand. These formulations, which will be discussed later in the paper, were derived by integration and differentiation of bending moment profiles recorded in lateral test results on centrifuge model piles and on a 368mm diameter pile installed in a test pit backfilled with sand from the Bass Strait, Australia. While these formulations provided a reasonable match to the experimental observations in the respective studies, their general applicability to the full range of sands types and pile diameters is unknown.

This paper addresses such uncertainty by using the Finite Element (FE) method to develop CPT based *p-y* relationships for piles in sand. The sand is assumed to be un-disturbed by the process of pile installation and is modelled as a non-linear elasto-plastic material. The interface between the pile and sand is assumed fully rough throughout. The responses of laterally loaded piles with a wide range of diameters in a variety of different sands are predicted in full 3D FE analyses. The corresponding CPT q_c profile for each sand is derived numerically using the same soil constitutive model via the cavity expansion analogue in a 2D axisymmetric FE analysis. An extensive series of computations predicting pile lateral response and CPT q_c values was performed for sands with different strengths and non-linear stiffness characteristics. These results are then used to formulate a direct method of constructing *p-y* curves from CPT q_c values. The proposed method is shown to be consistent with the 'power law' empirical relationship of Novello (1999) and to provide good predictions for the response recorded in lateral tests on field scales piles in an independent case study.

Numerical Approach

Constitutive Soil Model

A non-linear elasto-plastic constitutive model was employed to model the sand in the analyses. This model, which is referred to as the Hardening Soil (*HS*) model, is described by Schanz *et. al.* (1999). The model parameters are introduced in the following and their full descriptions as well as detailed explanations of the model including verification analyses are available at *www.plaxis.nl*:

- Stiffness varies with stress levels according to a power law, with an exponent (*m*) of 0.5 assumed for sand;
- Plastic straining due to shear loading occurs such that the Young's Modulus (E) in a drained triaxial test is given by the following hyperbolic relationship:

$$E = 2E_{50}\left(1 - R_f \frac{q}{q_f}\right) \; where \; E_{50} = \; {E_{50}}^{ref}\left(\frac{\sigma'_3}{p_{ref}}\right)^m \qquad (2)$$

  where q is the deviator stress, q_f is the maximum deviator stress, p_{ref} is the reference confining pressure, R_f is the failure ratio (set to 0.9 for this study) and E_{50}^{ref} is the E value at p_{ref} (which can be determined when q is 50% of q_f);
- Plastic straining due to primary compression is controlled by the 1D , stress-normalised, oedometric stiffness (E_{oed}^{ref}), which is usually similar in magnitude to E_{50}^{ref} (*www.plaxis.nl*);
- Elastic loading and unloading within the current yield surface is defined by a separate, stress normalised, modulus (E_{ur}^{ref}), which is typically about three times E_{50}^{ref} (*www.plaxis.nl*);
- Failure occurs in accordance to the Mohr-Coulomb failure criterion, where the critical state friction angle (ϕ_{cv}) is defined by the peak dilation angle (ψ) and friction angle (ϕ') as follows:

$$\sin \phi'_{cv} = \frac{\sin \phi' - \sin \psi}{1 - \sin \phi' \sin \psi} \qquad (3)$$

- The ratio of the plastic volumetric strain rate to plastic shear strain rate is sin ψ_m, where ψ_m is the mobilised dilation angle and can be obtained from Equation (3) by

setting ϕ' to the mobilised friction angle (ϕ_m). Plastic shear strains are derived by assuming that plastic volumetric changes are zero.

- Dilation ceases when the void ratio increases from its initial value (e_{init}) to a nominated maximum void ratio (e_{max}). This study assumed void ratio limits which are typical of sub-angular to sub-rounded uniformly graded sand (e_{max} = 0.78, e_{min} = 0.49).

Prediction of CPT q_c

Yu & Mitchell (1998) show that experimental q_c data can be predicted numerically to a good accuracy using cavity expansion theory. To model the penetration process, a spherical cavity expansion was simulated in the Plaxis 2D (version 2012) FE program, following similar procedures to those described in Xu & Lehane (2008). The limiting cavity pressure (p_{lim}) was measured and the value of q_c then derived using the following relationship proposed by Randolph et al. (1994):

$$q_c = p_{lim}(1 + \tan\phi' \tan 60^\circ) \quad (4)$$

A 2D axisymmetric FE mesh comprising 15-node triangular elements, similar to that described in Tolooiyan & Gavin (2011), was set up as shown in Figure 1. Vertical and horizontal fixities were applied to the base and horizontal fixity was applied to the left and right boundaries. The mesh is 10m wide and 21m deep, and comprised a 1m thick linear elastic dummy layer, a 20m thick weightless soil layer and a weightless linear elastic cavity cluster with a radius (a_o) of 0.1m. Spherical cavity expansion was simulated by applying positive volumetric strain to the cavity cluster and the cavity pressure–radial displacement

variation during expansion was deduced by averaging the output from selected displacement nodes and stress points around the cavity cluster. Cavity expansion analyses at different depths were performed by varying the unit weight of the dummy layer to generate the initial stress conditions in the soil layer corresponding to the desired depth. This technique minimizes the influence of boundary effects when simulating cavity expansion analyses at shallow depths.

To verify that the cavity expansion mesh has been set up correctly, the closed-form solutions of Yu & Houlsby (1991) were compared with the Plaxis 2D predictions for a Mohr–Coulomb soil model. For this calibration exercise, three spherical cavity expansions (MC1, MC2, MC3) were performed using the parameters listed in Table 1. Figure 2 shows that the Plaxis 2D predictions are in good agreement with the closed-form solutions. The differences between the closed-form and Plaxis 2D predictions for the limiting cavity pressure (p_{lim}) are minimal, with the greatest difference being only 1.3%, as shown in Table 2.

To verify the validity of using cavity expansion to predict CPT q_c, the q_c profile predicted from the FE analyses using the *HS* soil model was compared to CPT q_c profiles measured at a sand test bed site located at Blessington, County Wicklow (Tolooiyan & Gavin, 2011). A calibration procedure was undertaken using Plaxis 2D's SoilTest facility to find the optimised *HS* soil model parameters that yield the best fit between the model predictions and the laboratory oedometer and triaxial compression test results. The optimised parameters obtained from this calibration procedure are listed in Table 3, which differ

slightly from those described in Tolooiyan & Gavin (2011). A comparison of the FE model results using the optimised parameters and those described in Tolooiyan & Gavin (2011) can be seen in Figure 3. Using these optimised parameters, spherical cavity expansions were simulated to obtain the predicted CPT q_c profile at Blessington. This predicted profile is compared with measured q_c profiles on Figure 4 where it can be seen to provide a reasonable (but slight under-estimate) of the measured CPT q_c traces. The greater underestimation of the q_c predictions at shallow depths is potentially due to an under-estimate of the peak friction angle, which Doherty *et al.* (2012) estimate could be as high as 54°at 1m depth.

Prediction of Lateral Pile Response

The prediction of lateral pile response was obtained using the Plaxis 3D Foundation (version 2.2) FE program. A 3D finite element mesh comprising 15-node wedge elements was set up, as shown in Figure 5. Vertical and horizontal fixities were applied to the side boundaries. The mesh is 100m × 100m wide and 79m deep, and comprises a linear elastic, solid pile fully embedded at the centre of the mesh under a free head condition. No installation effects were considered (i.e. the pile was "wished into place") and hence the results can be considered more applicable to bored piles than to driven piles (although little distinction with respect to pile type is made in practice). The lateral soil resistance (*p*) is calculated as the first derivative of the pile shear force (Q) with respect to depth (z). The *p-y* variation during the load application was deduced by repeating the calculation of the soil resistance (*p*) at each load increment.

To verify the ability of the Plaxis 3D model to predict the lateral response of a pile using the *HS* constitutive model, calculations were performed using the mesh shown on Figure 5 (with all linear dimensions reduced by a factor of 2) for the Mustang Island field tests reported by Reese *et al*., (1974). The *HS* soil model parameters used for this verification exercise are listed in Table 4. The $E_{50}{}^{ref}$ (kPa) profile is assumed to be 25000*z* (where z is the depth in metres), which is equal to the equivalent linear soil stiffness profile proposed by Dodds & Martin (2007) for the Mustang Island test location. The variation of soil stiffness with depth was modelled in the FE analysis by dividing the soil profile into 22 1m thick uniform sand layers. Due to limited reported data on the sand, the friction angle was simply assumed to be the peak angle with a dilation angle of zero.

The predicted lateral pile load-displacement curve obtained in the FE analysis is shown on Figure 6 where it is seen to be a close match to the measured response. Figure 6 also shows that the pile bending moments at a selected lateral load level are very similar to those measured by Reese et al. (1974). The agreement evident on Figure 6 confirms that the numerical approach employed is suitable for the analysis of laterally loaded piles.

Finite Element Analyses

Dimensionless analysis indicated that the following relationship should be investigated for the parametric study of the FE results:

$$\frac{p}{\sigma'_v D} = f\left(\frac{q_c}{\sigma'_v}, \frac{y}{D}, \frac{z}{D}\right) \quad (5)$$

where D is the pile diameter, *p* is the calculated lateral resistance (per metre run) at depth, *z*, and displacement, *y*; q_c is the computed cone resistance and σ'_v is the vertical effective stress at depth, *z*.

A total of 110 FE analyses were carried out, comprising 100 lateral pile test simulations and 10 cavity expansion simulations. The test cases investigated are shown in Table 5, which comprises ten different sets of soil parameters and ten different pile diameters. All analyses assumed a dry sand condition (with soil unit weight, γ), a linear elastic (solid) pile and fully rough conditions at the pile-sand interface. The rather high upperbound ϕ'_{cv} employed of 40^o could represent that exhibited by angular carbonate sands (Lehane et al. 2012). The parameter range in Table 5 is generally consistent with the proposals of Al-Defae et al. (2013) for the HS model parameters applicable to sands.

The parameters listed in Table 6 were held constant to restrict the amount of computing required to a reasonable level. It is noted that while E_{oed}^{ref} and E_{ur}^{ref} were varied throughout the study, the analyses assumed fixed (but typical) ratios between these parameters and the selected E_{50}^{ref} value. The adopted E_{oed}/E_{50} ratio of unity is supported by validation exercises performed by Brinkgreve *et al.* (2010) although Al-Defae *et al.* (2013) propose a ratio of 1.25. Limitations of the HS model itself as well as the need to hold certain parameters constant (including γ) are recognised when assessing the precision of the relationships developed in the following. It is also noted that, as sand conditions were assumed dry, the term γz is used in the following to represent σ'_v in equation (5).

Post-processing of the lateral pile loading results involved double differentiation of the computed pile bending moments to derive the net pile lateral forces (p). The collated results comprised $\frac{p}{\gamma z D}$ values for z/D values between 0.4 and 4, and y/D values between 0.01 and 0.1 in soils with $\frac{q_c}{\gamma z}$ ratios between 38 and 400. It is noted that excluding effort involved in post-processing, each lateral pile loading analysis required 8 hours of computation time.

Power Law Relationship

The collated FE results were used initially to deduce the functional relationship between $\frac{p}{\gamma z D}$ and $\frac{q_c}{\gamma z}, \frac{y}{D}, \frac{z}{D}$ employing the power law format, similar to that used in the empirical CPT-based *p-y* relationships of Novello (1999) and Dyson & Randolph (2001). The functional form of the power law relationship is as follows:

$$\frac{p}{\gamma z D} = \mathrm{R}\left(\frac{q_c}{\gamma z}\right)^a \left(\frac{y}{D}\right)^b \left(\frac{z}{D}\right)^c \quad (6)$$

where R, a, b, c are unknown parameters

A non-linear regression analysis was carried out using the least squares method to determine these unknown parameters and this yielded the following best fit relationship:

$$\frac{p}{\gamma z D} = 4.2 \left(\frac{q_c}{\gamma z}\right)^{0.68} \left(\frac{y}{D}\right)^{0.56} \quad (7)$$

The $\frac{p}{\gamma z D}$ values calculated using Equation (7) for given $\frac{q_c}{\gamma z}$ *and* $\frac{y}{D}$ ratios are compared on Figure 7 with $\frac{p}{\gamma z D}$ values computed at the same ratios in the FE analyses. This comparison shows a reasonable fit to much of the FE computations although it is clear that certain estimates of $\frac{p}{\gamma z D}$ are over-predicted by nearly a factor of 2. These over-predictions correspond primarily with FE results at large y/D values.

Given that Equation (7) is based on the same power law framework as the existing CPT-based *p-y* relationships, a comparison between these relationships was carried out to identify any significant differences. To allow for a direct comparison, each relationship was rearranged into its component form, as shown in Table 7. The comparison shows that Equation (7) is in good agreement with the Novello (1999) relationship, which was derived largely on an intuitive basis from the backanalyses of centrifuge scale lateral load tests in calcareous sand. However, the empirical relationship proposed by Dyson & Randolph (2001), which was also assessed from centrifuge model pile tests in calcareous sand, predicts that *p* is independent of depth (*z*) and has a larger diameter dependence than the FE predictions; these differences can have a very significant impact on evaluated *p-y* curves.

Exponential Relationship

One major shortcoming of the power law relationship is its inability to model the limiting nature of the *p-y* curve. This limitation explains the tendency seen on Figure 7 for over-predictions at large displacements, but can be overcome easily with an exponential framework. The functional form of the exponential relationship is as follows:

$$\frac{p}{\gamma z D} = \frac{p_u}{\gamma z D}\left(1 - \exp(-\lambda)\right) \quad (8)$$

where $\frac{p_u}{\gamma\, z\, D}$ is the normalised ultimate soil resistance and λ is a soil stiffness decay coefficient. $\frac{p_u}{\gamma\, z\, D}$ should be independent of displacement and therefore a function only of $\frac{q_c}{\gamma\, z}$ and $\frac{z}{D}$. A review of the collated FE results indicated that the following power law format is a suitable functional form for both the normalized ultimate soil resistance and soil stiffness decay functions:

$$\frac{p_u}{\gamma z D} = \mathrm{R}_1 \left(\frac{q_c}{\gamma z}\right)^{a_1} \left(\frac{z}{D}\right)^{b_1} \quad (9)$$

$$\lambda = \mathrm{R}_2 \left(\frac{q_c}{\gamma z}\right)^{a_2} \left(\frac{z}{D}\right)^{b_2} \left(\frac{y}{D}\right)^{c_2} \quad (10)$$

where R_1, R_2, a_1, b_1, a_2, b_2, c_2 are unknown parameters

To determine the unknown parameters (R_1, R_2, a_1, b_1, a_2, b_2, c_2), non-linear regression analyses were carried out using the least squares method. These yielded the following best fit relationships:

$$\frac{p_u}{\gamma z D} = 2.4 \left(\frac{q_c}{\gamma z}\right)^{0.67} \left(\frac{z}{D}\right)^{0.75} \tag{11}$$

$$\lambda = 6.2 \left(\frac{z}{D}\right)^{-1.2} \left(\frac{y}{D}\right)^{0.89} \tag{12}$$

From Equation (7), the complete exponential relationship can then be determined as:

$$\frac{p}{\gamma z D} = 2.4 \left(\frac{q_c}{\gamma z}\right)^{0.67} \left(\frac{z}{D}\right)^{0.75} \left(1 - \exp\left(-6.2 \left(\frac{z}{D}\right)^{-1.2} \left(\frac{y}{D}\right)^{0.89}\right)\right) \tag{13}$$

Figure 8 compares the FE results with those calculated using Equation (13). Evidently, a good fit is obtained for all cases. A comparison of Figure 7 with Figure 8 provides an indication of the superior format of Equation (13) over Equation (7).

Field Test Validation

To assess the general applicability of Equation (13), the predicted lateral pile response obtained using *p-y* curves calculated using this equation was compared against the measurements obtained in an independent field study carried out in Hampton, Virginia (Pando *et al*. 2006). This field study included instrumented lateral tests in a medium dense silty sand on a prestressed concrete (PC) pile, a plastic pile (PP) and a fibre reinforced polymer (FRP) pile. Figure 9a shows the q_c profiles at the location of the FRP and PC piles; no CPT data are presented at the location of the PP pile but, based on their respective locations at the test site and inferences from assessed soil stiffness parameters given in Pando *et al.* (2006), it is assumed that ground conditions at the locations of the PC and PP

piles were very similar. The reported moment dependence of the flexural rigidity (EI) of each pile is presented on Figure 9b.

The geometries of the three test piles are summarised on Figure 10 which also shows the ground conditions and sand friction angles assessed by Pando *et al.* (2006). The *p-y* curves were derived using Equation (13) at depth intervals of 0.3m along the test piles and then input into the Oasys ALP program (Oasys 2010) to predict the lateral pile response. The square PC pile (of width 0.61m) was represented approximately as a pile with the same diameter. As for many other commercially available laterally loaded pile programs, the ALP program combines elastic beam elements and non-linear *p-y* springs to model lateral pile-soil interaction. The predictions needed to be performed in an iterative manner to ensure that the computed bending moments were consistent with the flexural rigidity characteristics shown on Figure 9b. Additional predictions for comparative purposes were also performed using *p-y* formulations recommended by API (2011) for the friction angles assessed by Pando et al. (2006), namely $\phi' = 33^o$ in the upper 10m and $\phi' = 35^o$ below 10m.

Figure 10 shows the comparison of the measured and predicted pile load-displacement curves at the original ground level. These predictions have been adjusted for the initial 'seating load' of 11kN applied in the field tests. It is clear from Figure 11 that predictions based on Equation (13) provide a very good match to the observed load displacement response. Figure 10 also shows that API (2011) predicts a stiffer load-displacement response from that measured; this is especially significant for the PC and PP piles.

Comparisons between the measured lateral pile deflection profiles and those predicted using the *p-y* curves derived using Equation (13) are presented on Figure 11 for three separate load levels. Encouragingly, it is evident that the calculated and measured profiles are very similar for all cases (apart from the under-prediction of displacements for the PC pile). This agreement provides additional corroboration in support of the general form of Equation (13) and the use of a direct CPT q_c approach for the analysis of laterally loaded piles in sand. Equation (13) has also been shown by the present authors (in a submission for the 3rd international symposium on cone penetration testing, which is being held in Las Vegas in May 2014, titled 'Verification of numerically derived CPT-based p–y curves for piles in sand') to lead to good predictions of other lateral pile load test data including tests in fully submerged conditions.

Conclusions

The difficulties in selecting appropriate stiffness and strength parameters for the prediction of lateral pile response prompted a numerical investigation of a CPT based *p-y* formulation for the analysis of laterally loaded piles in sand. The Finite Element computations performed to predict the q_c profiles and the *p-y* curves adjacent to laterally loaded piles (with diameters ranging from 0.5m to 5m) used the non-linear, elasto-plastic *HS* constitutive soil model. The computations involved q_c and *p-y* predictions in soils with a wide range of stiffnesses and strengths (as listed in Table 5), but the parameters listed in Table 6 were held constant so that overall computation time required for the study was realistic.

Regression analyses of the extensive series of computations, assuming a power law format, uncovered an expression (Equation 7) which is in good agreement with the empirical expression derived by Novello (1999) using experimental data for laterally loaded piles in calcareous sand. An improved exponential format for *p-y* curves is proposed (Equation 13), which is shown to provide a better match to the computations as well as incorporating the tendency for lateral pressures to reach a limiting or ultimate value. The applicability of Equation (13) to laterally load tests in the field is verified by the good predictive match obtained with the measured response of three piles in Hampton sand.

Equation (13) provides important insights into the relative effects of various parameters controlling p-y curves in sand. Withstanding the simplifications involved in its derivation, the paper provides strong support for a changeover to a CPT q_c based *p-y* formulation for sands. It is hoped that additional calibration against more case history data will assist with the refinement of Equation (13).

Notation

a	current radius of spherical cavity
a_0	initial radius of spherical cavity
c'	cohesion
CPT	cone penetration test
D	pile diameter
D_r	relative density
e_{init}	initial void ratio
e_{min}	minimum void ratio
e_{max}	maximum void ratio
E	drained secant Young's modulus
E_{50}^{ref}	E value determined when q = 50% of q_f at p_{ref}
E_{oed}^{ref}	oedometer loading modulus at p_{ref}
E_{ur}^{ref}	unloading modulus at p_{ref}
K_0	earth pressure coefficient
L	pile length
m	exponent controlling the stress level dependence of stiffness
p	lateral soil resistance per unit pile length
p_{lim}	cavity expansion limit pressure
p_{ref}	reference confining pressure
q	deviator stress
q_f	maximum deviator stress

q_c	steady state penetration resistance
R_f	failure ratio
y	local pile displacement
z	depth below ground surface
σ'_{h0}	in-situ horizontal stress
σ'_v	Vertical effective stress (at depth, z)
γ	Soil unit weight
γ_{pile}	Pile unit weight
ϕ'	peak friction angle
ϕ'_{cv}	constant volume friction angle
ψ	dilation angle
ν	Poissons ratio

References

Al-Defae A.H., Caucis K. and Knappett J.A. (2013). Aftershocks and the whole-life seismic performance of granular slopes. *Géotechnique* **63**, No. 14, 1230–1244.

American Petroleum Institute (2011). Part 4: Geotechnical and Foundation Design Considerations. ANSI/API Recommended Practice 2GEO, 1st Edition, April 2011. Thomson Scientific, US.

Broms B.B. (1964). Lateral resistance of piles in cohesionless soils. *Journal Soil Mechanics and Foundation Div.*, 90, No. 3, 123-158.

Brinkgreve R.B.J., Engin E. and Engin H.K. (2010). Validation of empirical formulas to derive model parameters for sand. In *Numerical Methods in geotechnical engineering* (eds T. Benz and S. Nordal), pp 137-142. Rotterdam, The Netherlands: CRC Press/Balkema.

Doherty P., Kirwan L., Gavin K., Igoe D., Tyrrell S., Ward D. & O'Kelly B. Soil properties at the UCD geotechnical research site at Blessington. *Bridge and Concrete Research in Ireland 2012, Ireland*.

Dodds A. & Martin G. Modeling Pile Behavior in Large Pile Groups under Lateral Loading. *Report to MCEER*, April 2007.

Dyson, G. J. & Randolph, M. F. (2001). Monotonic Lateral Loading of Piles in Calcareous Sand. *Journal of Geotechnical and Geoenvironmental Engineering* **127**, No. 4, 346–352.

Houlsby, G. T. & Hitchman, R. (1988). Calibration chamber tests of a cone penetrometer in sand, *Géotechnique* **38**, No. 1, 39–44.

Lee J., Kim M. and Kyung D. (2010). Estimation of lateral load capacity of rigid short piles in sands using CPT results. *Journal of Geotechnical and Geoenvironmental* Engineering, ASCE, 136, No. 1, 48-56.

Lehane, B.M., Schneider J.A., Lim J.K. and Mortara, G. (2012). Shaft friction from instrumented displacement piles in an uncemented calcareous sand. J. Geotechnical & Geoenvironmental Engrg., **138**, No. 11, 1357-1368..

Novello, E. A. (1999). From static to cyclic p-y data in calcareous sediments *Engineering for calcareous sediments* **1**, 17–24.

O'Neill M. W. & Murchinson J. M. (1983). An evaluation of p-y relationships in sands. *Report to American Petroleum Institute*, May 1983.

Oasys (2010). Geotechnical Software., ALP manual, *www.oasys-software.com*, UK.

Pando M.A., Ealy C.D., FILz G.M., F., Lesko J.J., & Hoppe E.J. (2006). A Laboratory and Field Study of Composite Piles for Bridge Substructures. *Report to Virginia Transportation Research Council*, March 2006.

Randolph, M. F., Dolwin, J. & Beck, R. (1994). Design of driven piles in sand. *Géotechnique* **44**, No. 3, 427–448.

Reese, L. C., Cox, W. R. & Koop, F. D. (1974). Analysis of laterally loaded piles in sand. *6th Offshore Technology Conference, Houston, Texas.*

Salgado, R. & Randolph, M. F. (2001). Analysis of Cavity Expansion in Sand. *International Journal of Geomechanics* **1**, No. 2, 175–192.

Schanz, T., Vermeer, P. A. & Bonnier, P. G. (1999). The hardening soil model: formulation and verification. In *Beyond 2000 in computational geotechnics: 10 Years of Plaxis*, 1–16.

Tolooiyan A. & Gavin K. (2011). Modelling the Cone Penetration Test in sand using Cavity Expansion and Arbitrary Lagrangian Eulerian Finite Element Methods. *Computers and Geotechnics* **38**, No. 1, 482–490.

Vesic, A. S. (1961). Beams on Elastic Subgrade and the Winkler Hypothesis, *5th Int Conf. Soil Mech Found Engrg.*, **1**, Paris.

Xu, X. & Lehane, B. M. (2008). Pile and penetrometer end bearing resistance in two layered soil. *Géotechnique* **58**, No. 3, 187–197.

Yu, H. S. & Houlsby, G. T. (1991). Finite cavity expansion in dilatant soils: loading analysis. *Géotechnique* **41**, No. 2, 173–183.

Yu, H. S. & Mitchell, J. K. (1998). Analysis of cone resistance: review of methods. *Journal of Geotechnical and Geoenvironmental Engineering* **124**, No. 2, 140–149.

FIGURES

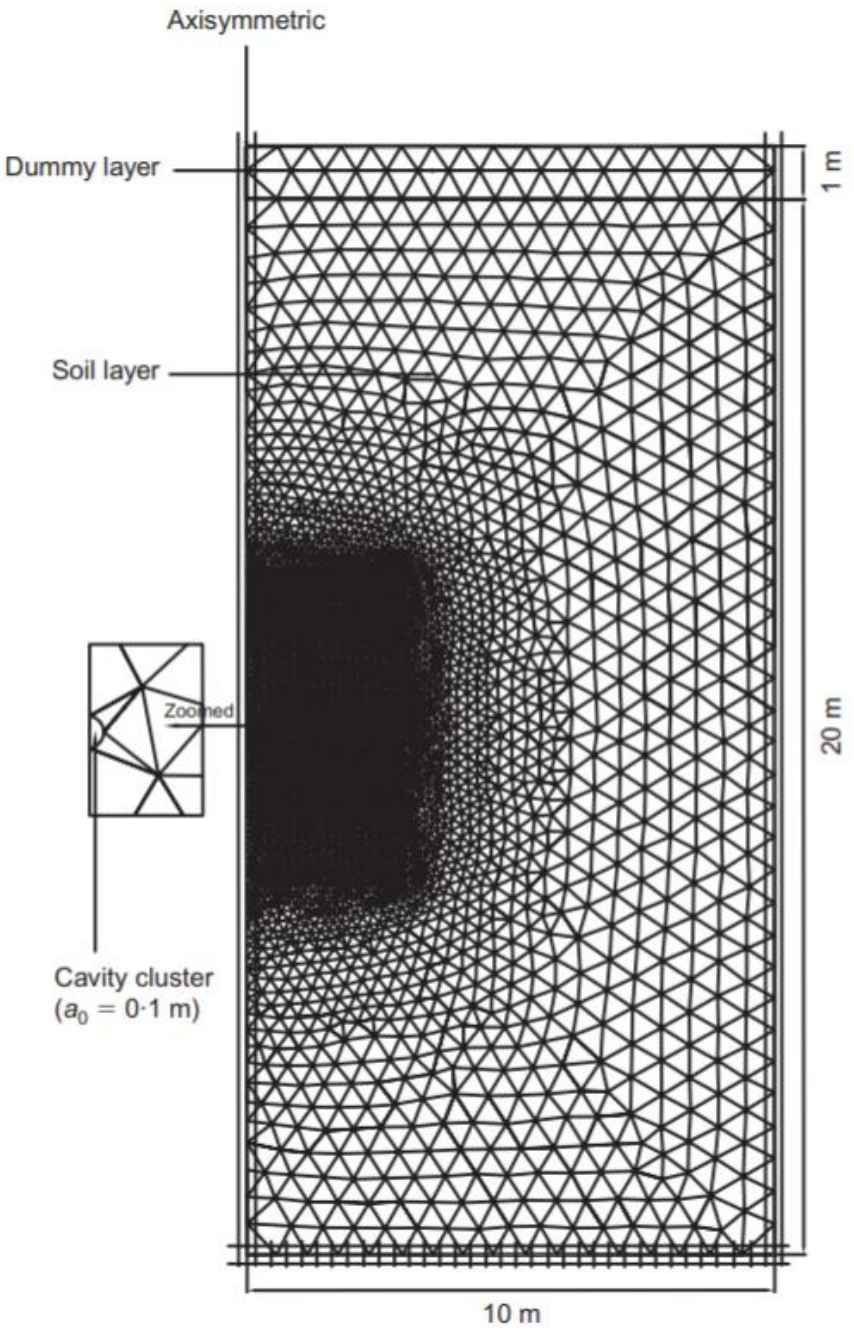

Figure 1: Spherical cavity expansion mesh (Plaxis 2D)

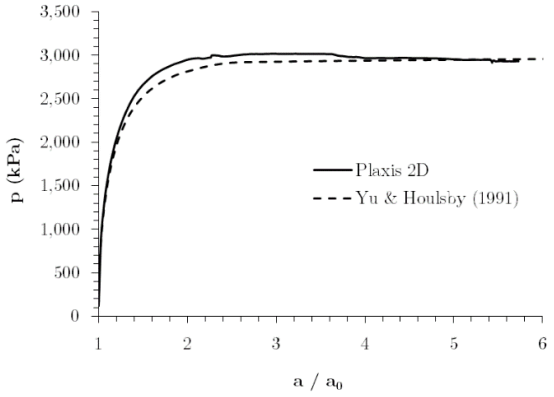

(a)

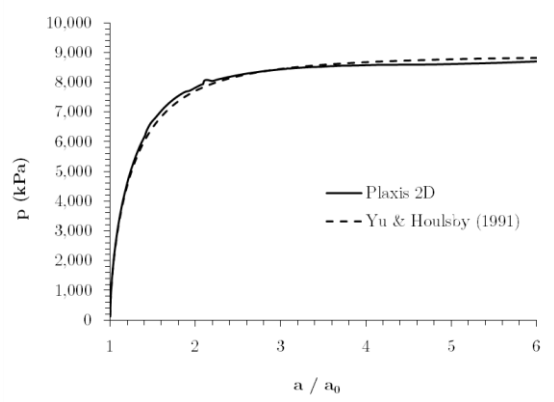

(b)

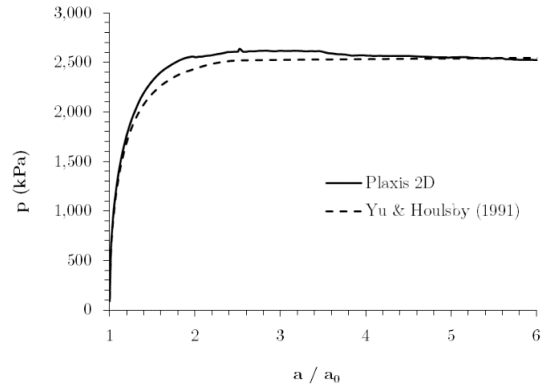

(c)

Figure 2: Comparison of Plaxis 2D results for (a) MC1, (b) MC2 and (c) MC3 with closed form solutions (Yu & Houlsby, 1991)

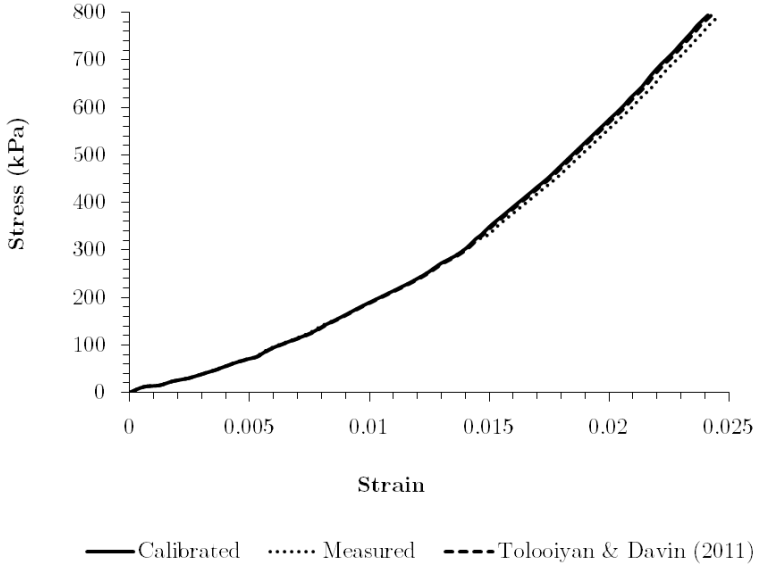

(a)

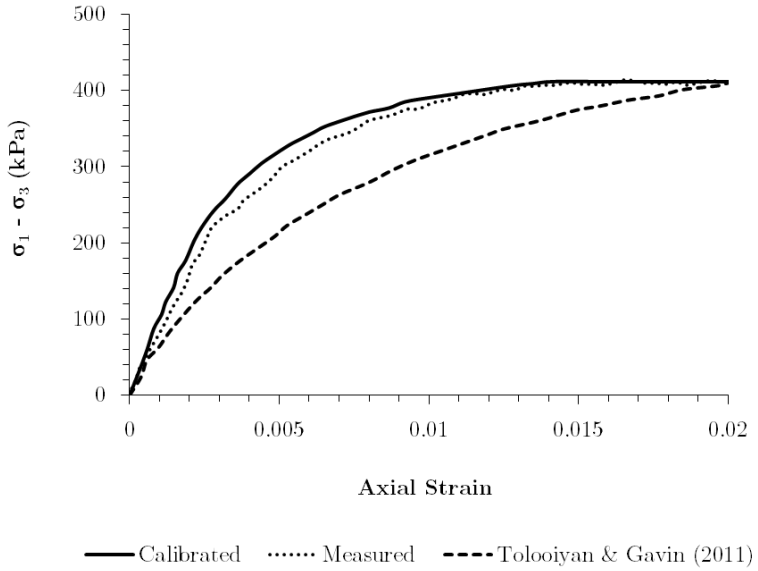

(b)

Figure 3: Comparison of FE calibration results of (a) oedometer test and (b) triaxial compression test with laboratory measurements

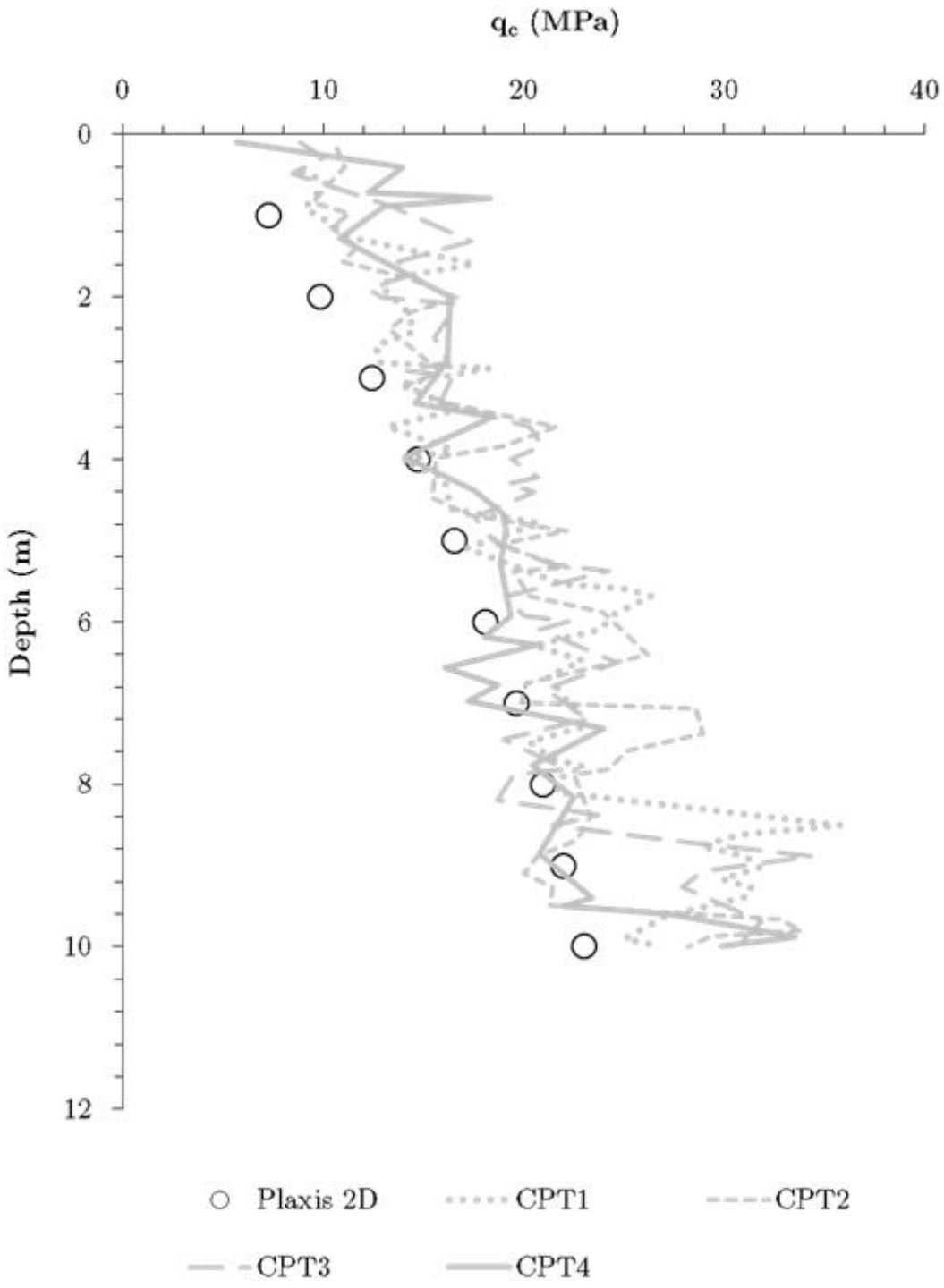

Figure 4: Comparison of Plaxis 2D predictions against field measurements

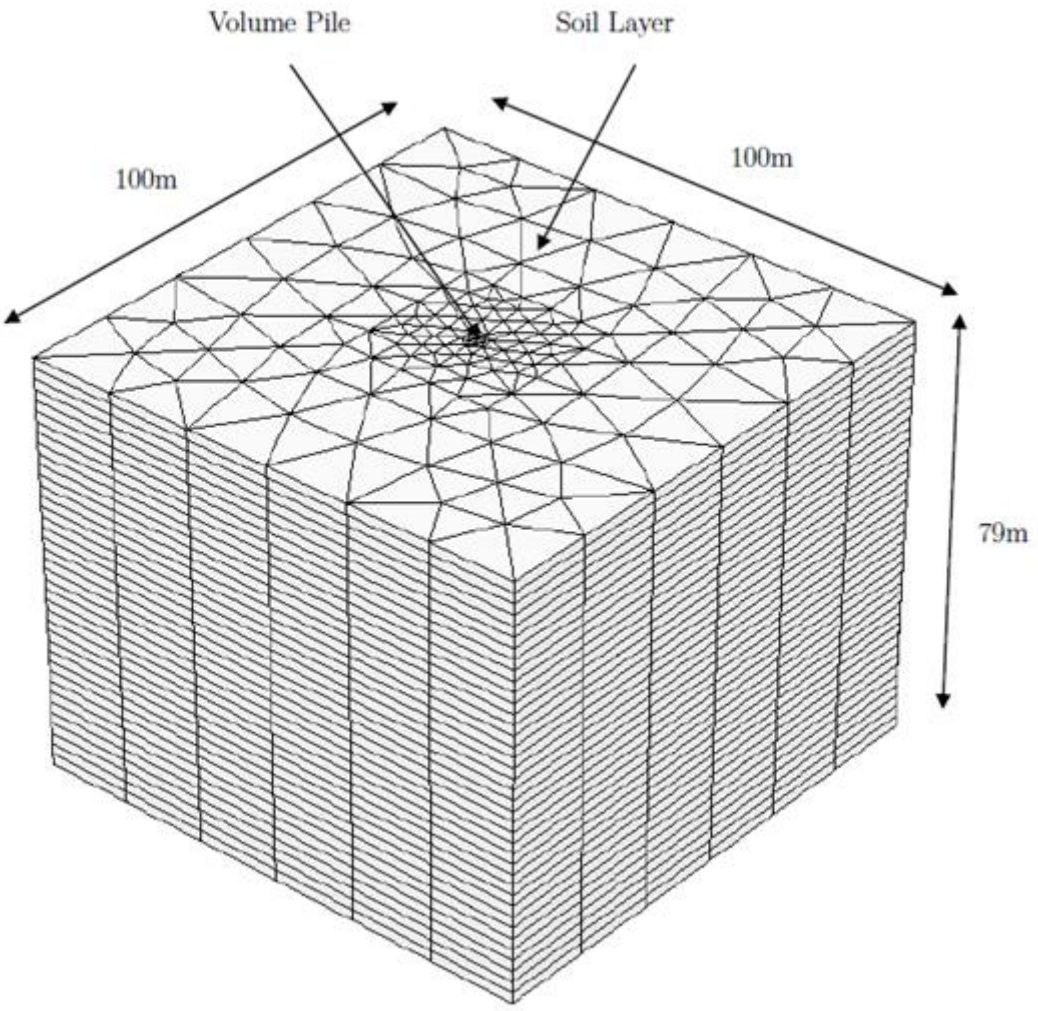

Figure 5: Lateral pile test mesh (Plaxis 3D Foundation)

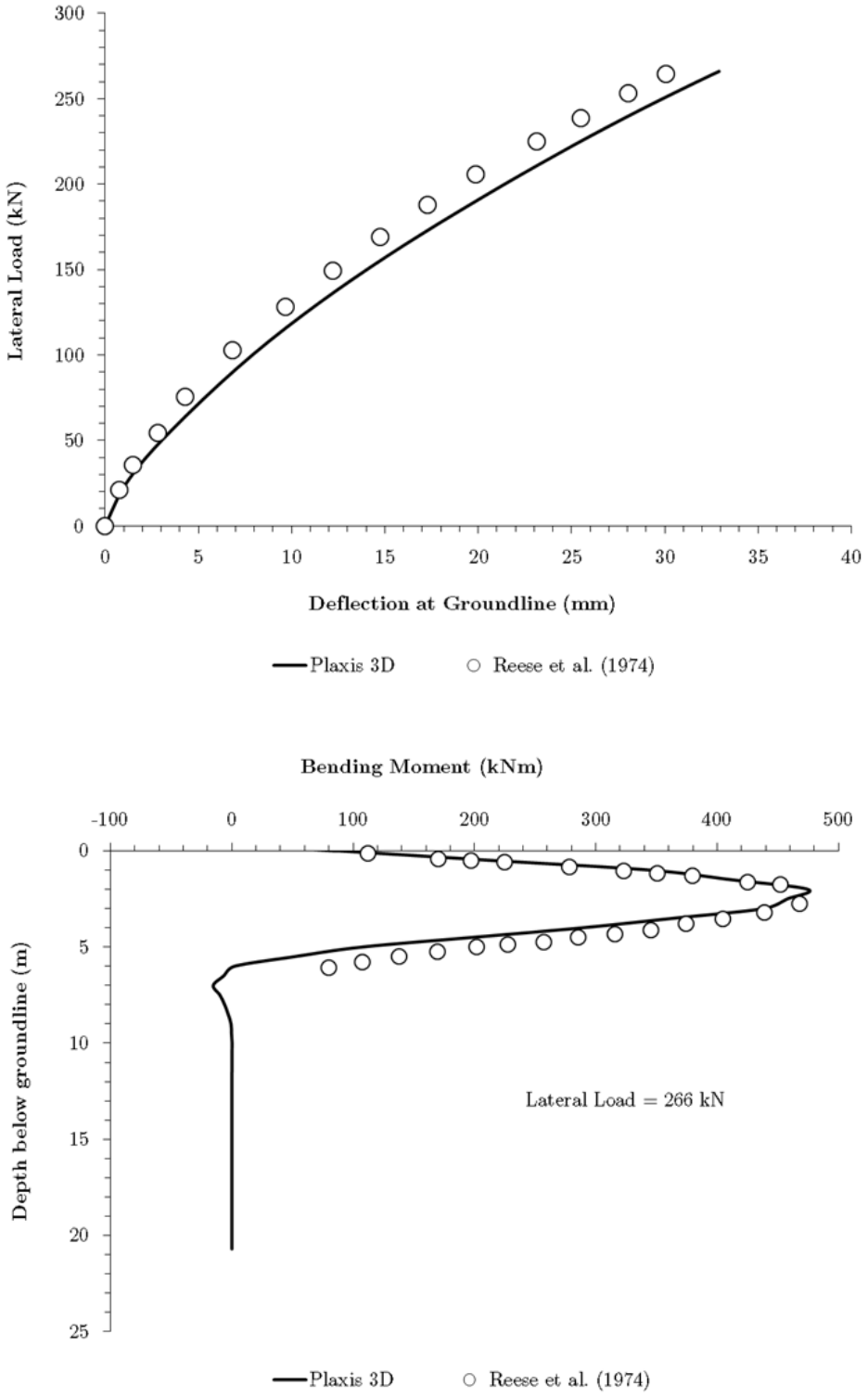

Figure 6: Comparison of FE predictions of pile displacements and bending moments with and field measurements of Reese *et al.* (1974).

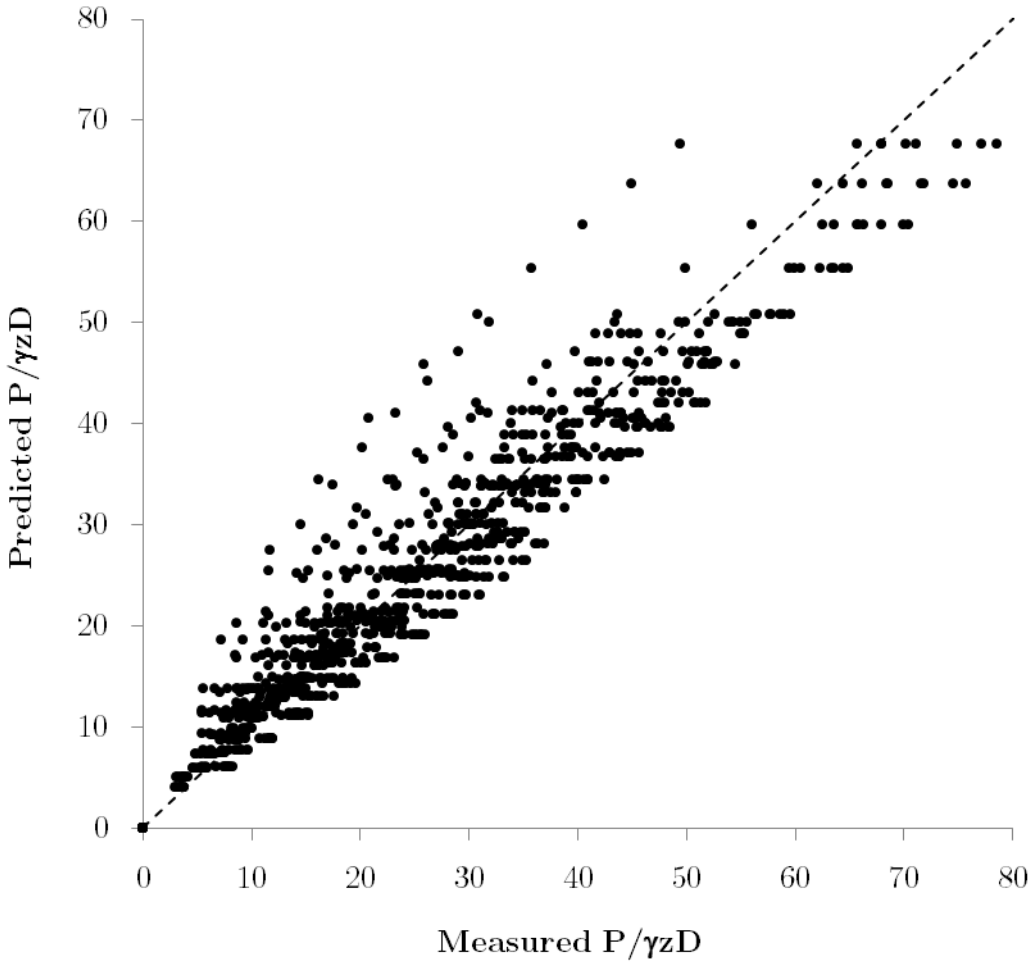

Figure 7: Comparison between FE results and predictions obtained using Equation (7)

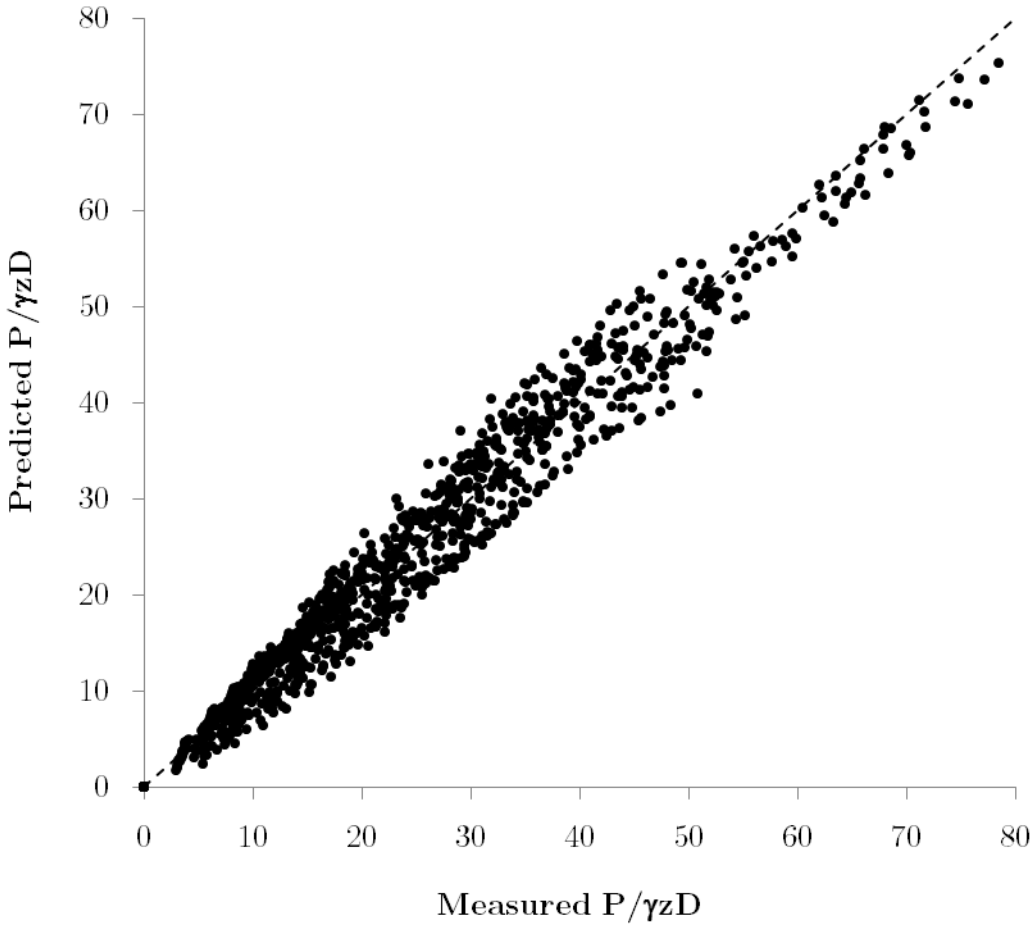

Figure 8: Comparison between FE results and predictions obtained using Equation (13)

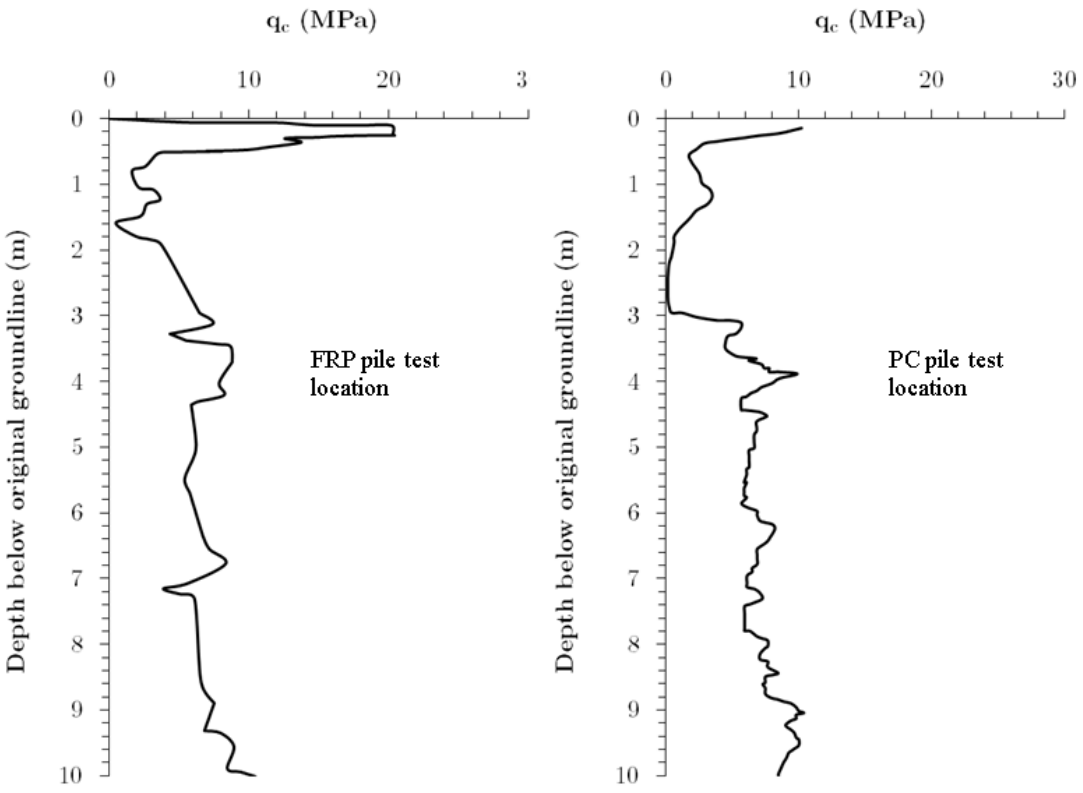

(a)

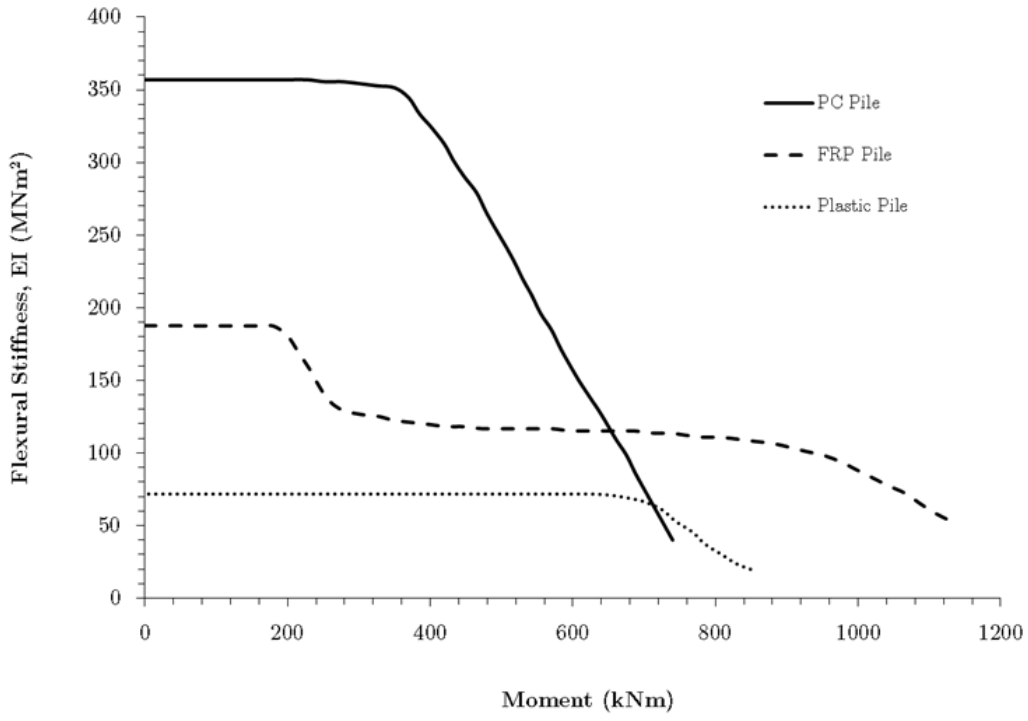

(b)

Figure 9: (a) CPT qc at test pile locations, (b) flexural characteristics of the test piles (Pando *et al*., 2006)

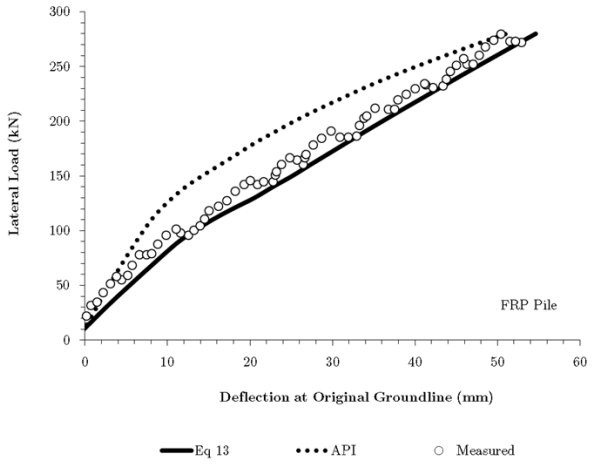

(a)

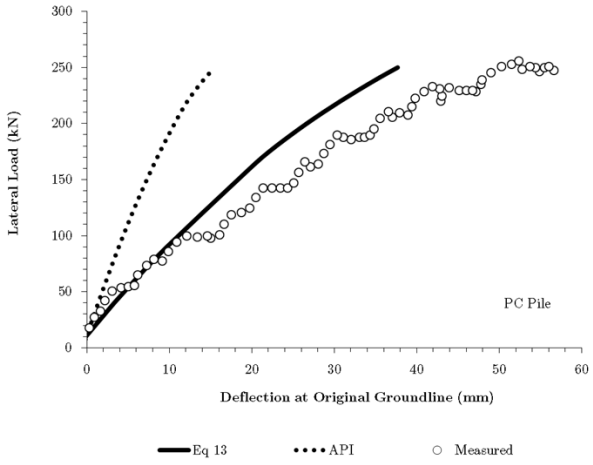

(b)

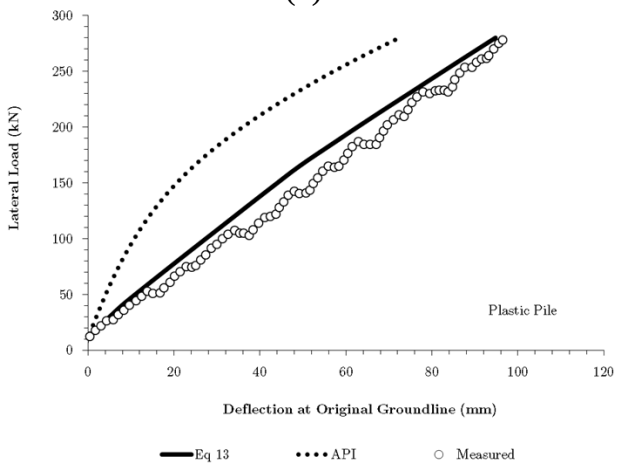

(c)

Figure 10: Predicted and measured pile head load–displacement curves at Hampton, Virginia, USA: (a) FRP pile; (b) PC pile; (c) plastic pile

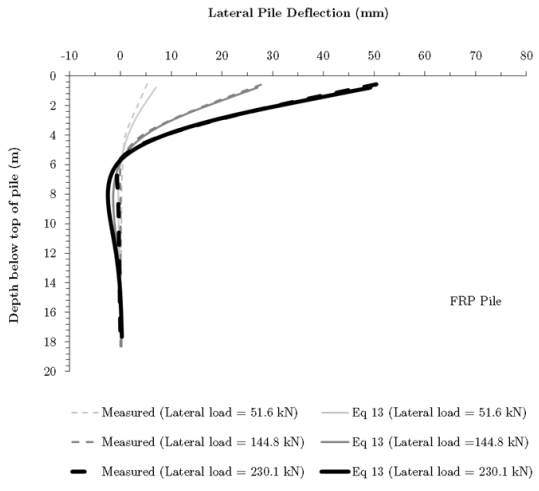

(a)

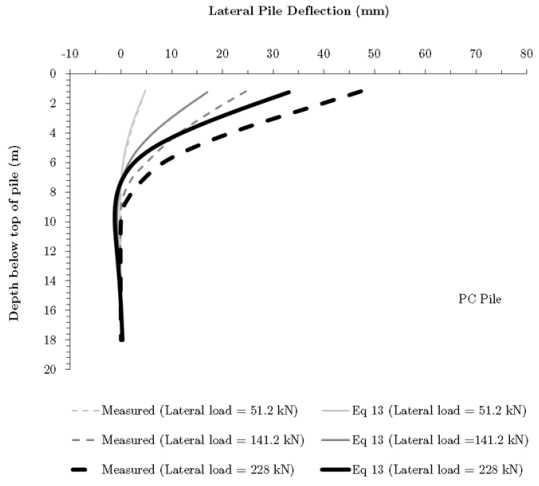

(b)

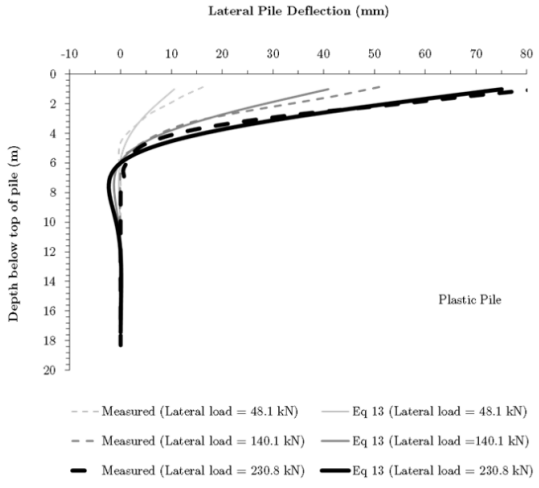

(c)

Figure 11: Predicted and measured displacement profiles at Hampton, Virginia: (a) FRP pile; (b) PC pile; (c) plastic pile

TABLES

Table 1: Material parameters for FE cavity expansion verification

	p_0 (kPa)	E (MPa)	ν	c’	ϕ' (^{o})	ψ (^{o})
MC1	120	50	0.2	0.2	40	0
MC2	120	100	0.2	0.2	42	12
MC3	90	50	0.2	0.2	40	0

Table 2: Summary of FE cavity expansion verification results

	p_o (kPa)	p_1 (Closed-form)	p_2 (Plaxis 2D)	$(p_2 - p_1)/p_1$ (%)
MC1	120	3006	3018	0.40
MC2	120	8908	8819	-1.0
MC3	90	2602	2637	1.3

Table 3: Material parameters for FE q_c predictions verification

Property	Value
Material Type	Hardening Soil
Drainage Type	Drained
E_{50}^{ref} (kPa)	97000
E_{oed}^{ref} (kPa)	25000
E_{ur}^{ref} (kPa)	200000
γ_{unsat} (kN/m^3)	20
ϕ' (^{o})	42.4
c'	0
ψ (^{o})	6.6
ν	0.2
m	0.5
R_f	0.9
Tensile Strength (kPa)	0
e_{init}	0.373
e_{min}	0.373
e_{max}	0.733
p_{ref} (kPa)	100

Table 4: Material parameters for FE lateral pile response predictions verification

(a) Soil Parameters

Property	Value
Material Type	Hardening Soil
Drainage Type	Drained
E_{50}^{ref} (kPa)	25000z (z=depth in metres)
E_{oed}^{ref}	E_{50}
E_{ur}^{ref}	$3E_{50}$
γ_{sat} (kN/m^3)	20.4
ϕ' (^{o})	39
c'	0
ψ (^{o})	0
ν	0.33
Phreatic Level (m)	0

(b) Pile parameters

Property	Value
Pile Type	Massive Circular
Material Type	Linear Elastic
Drainage Type	Non-porous
$E_{p\text{-}equivalent}$ (kPa)	2.4×10^7
ν	0.25
D (m)	0.61
L (m)	21

Table 5: Test cases investigated in the numerical study

e_{init}	D_r	E_{50}^{ref} (MPa)	ϕ' (^{o})	ψ (^{o})	ϕ'_{cv} (^{o})	Pile Diameters (m)
0.5	0.97	100	43.9	15	32	0.5, 1, 1.5, 2, 2.5, 3, 3.5, 4, 4.5, 5
0.5	0.97	100	50.6	15	40	0.5, 1, 1.5, 2, 2.5, 3, 3.5, 4, 4.5, 5
0.5	0.97	60	43.9	15	32	0.5, 1, 1.5, 2, 2.5, 3, 3.5, 4, 4.5, 5
0.5	0.97	60	50.6	15	40	0.5, 1, 1.5, 2, 2.5, 3, 3.5, 4, 4.5, 5
0.6	0.62	60	41.7	12	32	0.5, 1, 1.5, 2, 2.5, 3, 3.5, 4, 4.5, 5
0.6	0.62	60	48.6	12	40	0.5, 1, 1.5, 2, 2.5, 3, 3.5, 4, 4.5, 5
0.7	0.28	60	36.1	5	32	0.5, 1, 1.5, 2, 2.5, 3, 3.5, 4, 4.5, 5
0.7	0.28	60	43.7	5	40	0.5, 1, 1.5, 2, 2.5, 3, 3.5, 4, 4.5, 5
0.7	0.28	20	36.1	5	32	0.5, 1, 1.5, 2, 2.5, 3, 3.5, 4, 4.5, 5
0.7	0.28	20	43.7	5	40	0.5, 1, 1.5, 2, 2.5, 3, 3.5, 4, 4.5, 5

Table 6: Constant parameters for all test cases

(a) Soil Parameters

Property	Value
K_o	0.45
ν	0.2
c'	0
γ	18 kN/m^3
e_{max}	0.78
e_{min}	0.49
E_{oed}^{ref}	E_{50}^{ref}
E_{ur}^{ref}	$3E_{50}^{ref}$

(b) Pile Parameters

Property	Value
γ_{pile}	24 kN/m^3
ν	0.2

Table 7: CPT-based *p-y* relationships

Relationship	Equation (Original form)	Equation (Component form)
Equation (7)	$\frac{p}{\gamma z D} = 4.2\left(\frac{q_c}{\gamma z}\right)^{0.68}\left(\frac{y}{D}\right)^{0.56}$	$p = 4.2\,(q_c)^{0.68}\,(z)^{0.32}\,(y)^{0.56}(\gamma)^{0.32}\,(D)^{0.44}$
Novello (1999)	$\frac{p}{D} = 2\,(\gamma z)^{0.33}(q_c)^{0.67}\left(\frac{y}{D}\right)^{0.5}$	$p = 2\,(q_c)^{0.67}\,(z)^{0.33}\,(y)^{0.5}(\gamma)^{0.33}\,(D)^{0.5}$
Dyson & Randolph (2001)* * R factor for preinstalled piles	$\frac{p}{\gamma D^2} = 1.35\left(\frac{q_c}{\gamma D}\right)^{0.72}\left(\frac{y}{D}\right)^{0.58}$	$p = 1.35\,(q_c)^{0.72}\,(z)^{0}\,(y)^{0.58}(\gamma)^{0.28}\,(D)^{0.7}$